Updated version 8 November 2024

Assembly, integration, and laboratory testing of the EXCITE spectrograph

Lee Bernard[1], Johnathan Gamaunt[1], Logan Jensen[1], Andrea Bocchieri[2], Nat Butler[1], Quentin Changeat[3], Azzurra D'Alessandro[13], Billy Edwards[3], Conor Earley[1], Qian Gong[4], John Hartley[5], Kyle Helson[4, 12], Daniel P. Kelly[4], Kanchita Klangboonkrong[6], Annalies Kleyheeg[6], Nikole Lewis[7], Steven Li[5], Michael Line[1], Stephen F. Maher[4], Ryan McClelland[4], Laddawan R. Miko[4], Lorenzo V. Mugnai[2, 8], Peter Nagler[4], C. Barth Netterfield[9], Vivien Parmentier[10], Enzo Pascale[2], Jennifer Patience[1], Tim Rehm[6], Javier Romualdez[5], Subhajit Sarkar[11], Paul Scowen[4,1], Gregory S. Tucker[6], Augustyn Waczynski[4], and Ingo Waldmann[3]

[1]School of Earth and Space Exploration, Arizona State University, Tempe AZ, USA
[2]Department of Physics, La Sapienza Università di Roma, Roma, Italy
[3]Department of Physics, University College London, London, UK
[4]NASA Goddard Space Flight Center, Greenbelt MD, USA
[5]StarSpec Technologies Inc., Cambridge Ontario, Canada
[6]Department of Physics, Brown University, Providence RI, USA
[7]Department of Astronomy, Cornell Univ., Ithaca NY, USA
[8]INAF – Palermo Astronomical Observatory, Piazza del Parlamento, Italy
[9]Department of Physics, Univ of Toronto, Toronto Ontario, Canada
[10]Department of Physics, AOPP, Univ. of Oxford, Oxford, UK
[11]School of Physics and Astronomy, Cardiff Univ., Cardiff, UK
[12]Center for Space Sciences and Technology, University of Maryland, Baltimore MD, USA
[13]Centre for ExoLife Sciences, University of Copenhagen, Copenhagen, Denmark

ABSTRACT

The EXoplanet Climate Infrared TElescope (EXCITE) is a near-infrared spectrograph (0.8-3.5 μm, R∼50) designed for measuring spectroscopic phase curves of transiting hot Jupiter-type exoplanets that operates off a high-altitude balloon platform. Phase curves produce a combination of phase curve and transit/eclipse spectroscopy, providing a wealth of information for characterizing exoplanet atmospheres. EXCITE will be a first-of-kind dedicated telescope uniquely able to observe a target nearly uninterrupted for tens of hours, enabling phase curve measurements, and complementing JWST. The spectrometer has two channels, a 0.8-2.5 μm band and a 2.5-3.5 μm band, providing a spectrum with a spectral resolution of R≥50. Two Off-Axis Parabolic (OAP) mirrors reimage the telescope focal plane to provide on-axis, diffraction-limited performance, wth a CaF_2 prism providing dispersion. The spectrum is imaged with a single JWST flight spare Teledyne H2RG detector, providing Nyquist sampling of each channel. Here, we discuss the spectrograph's mechanical design, acceptance testing, assembly, and cryostat integration.

Keywords: Exoplanet spectroscopy, hot Jupiters, balloon-borne instrumentation, infrared instrumentation

1. INTRODUCTION

The EXoplanet Climate Infrared TElescope (EXCITE)[1] is a NASA-funded high-altitude long-duration balloon flight infrared spectrograph (0.8-3.5 μm, R∼50) designed for measuring spectroscopic phase curves of transiting

Further Author Information:
Lee Bernard: ldbernard@asu.edu
Johnathan Gamaunt: jgamaunt@asu.edu

Ground-based and Airborne Instrumentation for Astronomy X, edited by Julia J. Bryant, Kentaro Motohara, Joël R. D. Vernet, Proc. of SPIE Vol. 13096, 13096A5
 · 0277-786X · doi: 10.1117/12.3019286

hot Jupiter-type exoplanets. Phase curves produce a combination of phase curve and transit/eclipse spectroscopy, providing a wealth of information for characterizing exoplanet atmospheres, but require long observation stares that consume the limited resources of shared observatories such as JWST. EXCITE will be a first-of-kind dedicated telescope uniquely able to observe a target nearly uninterrupted for tens of hours, enabling phase curve measurements and complementing JWST.

This paper is an update to and continuation of our previous paper on EXCITE's spectrograph design, Bernard et al 2022.[2] An overview of the EXCITE mission can be found in Nagler et al 2022.[1] Updates on the cryostat status can be found in Kleyheeg et al.[3] and updates on the gondola pointing system can be found in Romualdez et al.[4] Here, we discuss thermal simulations and tolerances of the spectrograph, and the design changes we made as a consequence of the simulation results. We also discuss the optics acceptance testing, assembly of the spectrograph and spectrograph alignment, as well as integration with the cryostat and telescope flight package. Finally, we discuss preparations for future engineering testing and test flights.

1.1 Summary of the Spectrograph Design

This two-channel, large range low-resolution spectrograph (**Figure 1**) (short channel 0.8-2.5 μm, long channel 2.5-3.5 μm, R≥50) makes use of a 0.5 meter-class telescope on a high-altitude balloon flight platform. The telescope produces a $f/12$ infrared (> 0.8 μm) beam, illuminating a cryogenic (120 K) 100-micron wide field stop. Cryogenic optics collimate the beam from the field stop, which is then directed through a cold stop to reduce stray light. A CaF_2 prism provides dispersion, and the camera optic focuses the dispersed beam through a dichroic (cutoff 2.5 μm), splitting the beam into short and long wavelength channels. A short pass filter operating at 65 K in the front of the detector package defines the band stop by eliminating light longward of 3.5 μm, and the focal plane is imaged by an H2RG detector.

This on-axis instrument makes use of Off-Axis Parabolic Mirrors (OAPs), providing efficient throughput in a compact design. A 45° OAP with a focal length $f = 101.6$ mm provides the collimation, and is followed by a 30° OAP with $f = 272.2$ mm providing camera focus. The combination of the optics magnifies the beam ($f/32.2$ effective) to achieve near optimal spatial sampling at the detector, with fold mirrors maintaining a 30.5 cm (12 inch) diameter envelope. All mirrors and the prism are off-the-shelf parts.

2. MECHANICAL DESIGN

2.1 Mechanical Redesign

The spectrograph mechanical design revolves around the optics bench, providing a stable platform for the optics and interfacing with the cryostat cold plate. The key design requirement of the spectrograph was maintaining the beam path length. The total beam path length from when the light enters the spectrograph slit to when it lands on the detector can change as much as 0.77 mm from when the instrument is at room temperature to when it is operating at 120 K.

The optics bench was originally set to be made of 6061-T6 aluminum. We quickly determined that aluminum had a CTE that was much too large, and the beam path would shorten by approximately 1.21 mm due to the optics bench shrinking. To assess the dimensional changes of the optics bench, we utilized the linear thermal expansion equation

$$dL = L_0 \, \alpha \, dT \tag{1}$$

We applied this equation, which governs how an object's length changes with temperature variation, to determine the change in length (dL) based on the initial length (L_0), the coefficient of thermal expansion (α), and the temperature change (dT). At room temperature, 6061 aluminum exhibits a CTE of 23.6×10^{-6} °C^{-1}.[5] With a temperature change of 193 K, this would lead to a contraction in the diameter of the optics bench by approximately 1.21 mm, consequently shortening the beam path by a similar amount. By contrast, titanium 6Al-4V boasts a CTE of 8.8×10^{-6} °C^{-1},[5] resulting in a diameter contraction of about 0.46 mm when subjected to the same temperature change. This leaves a margin of 0.31 mm, illustrating titanium's ability to better maintain dimensional stability under varying temperature conditions.

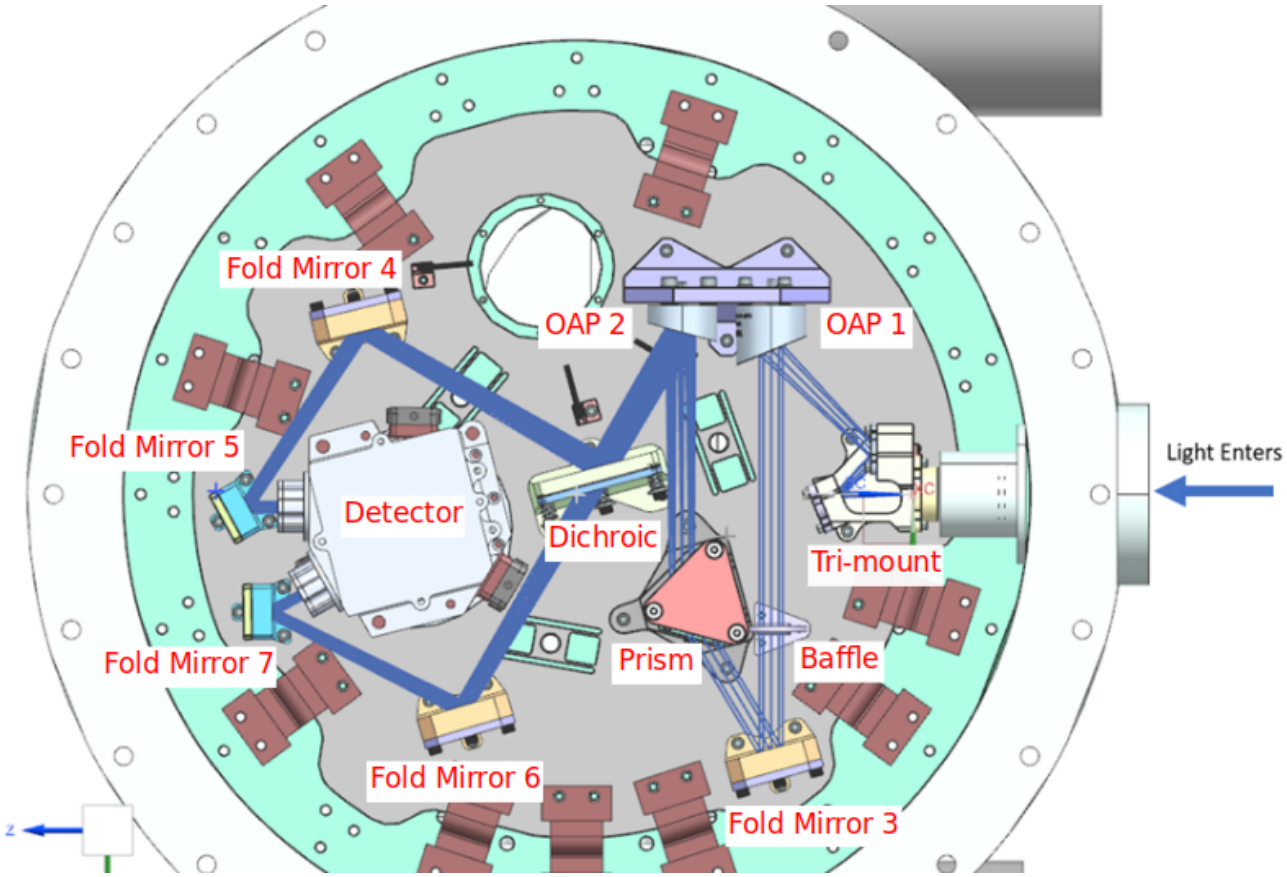

Figure 1: Top-down view of the EXCITE mechanical drawing.
The blue lines represent the optical ray-trace. Light enters from the right side of the spectrograph via a 100 µm wide by 3 mm tall field stop in the **Tri-mount**. The Tri-mount holds the Field Stop, as well as Fold Mirror 1 and Fold Mirror 2, which direct light into the collimating optic, **OAP 1**. **Fold Mirror 3** directs collimated light through the dispersing CaF_2 **Prism** and into the camera optic, **OAP 2**. Channel 1 (0.8-2.5 µm) is reflected by the **Dichroic** and directed by **Fold mirrors 4** and **5** into the detector box. Channel 2 (2.5-3.5 µm) is directed by **Fold Mirrors 6** and **7**. Short pass filters on the detector box define the 3.5 µm bandstop, and in both channels prevent unwanted thermal light from reaching the detector. The **Baffle** between OAP 1 and Fold Mirror 3 blocks stray light. Note how OAP 1 and OAP 2 make use of the same mount to ensure they are co-aligned.

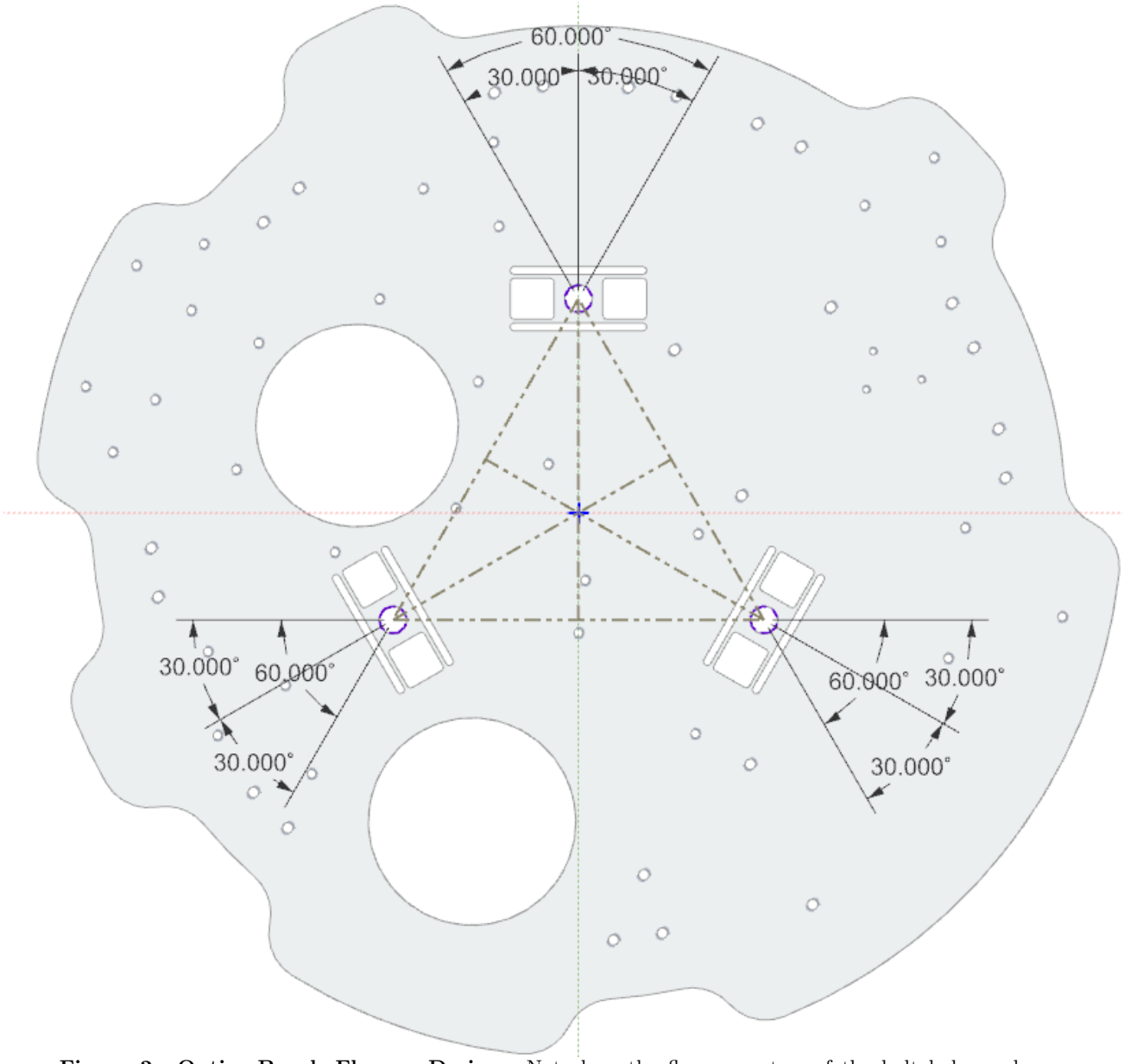

Figure 2: Optics Bench Flexure Design. Note how the flexure centers of the bolt holes make an equilateral triangle. The flexures are oriented perpendicular to the reference line bisecting each corner of the equilateral triangle. The reference lines bisecting the corners intersect at the middle of the optics bench keeping the center of the optics bench stationary during temperature fluctuations.

2.1.1 Flexture Design

The interface between the cold plate and the optics bench is crucial as it serves as the primary means of cooling the optics assembly. However, this interface poses potential challenges due to the substantial CTE mismatch, with the cold plate being made of aluminum. Such a mismatch could result in significant stresses at the interface, leading to warping or even failure. To address this issue, we designed flexures (**Figure 2**) to be precisely machined into the titanium optics bench. Strategically positioned around the center of the optics bench, the screw hole centers form an equilateral triangle configuration. Perpendicular to the reference lines bisecting each corner of the triangle, these flexures effectively manage stresses. Their intersection at the optics bench's midpoint ensures stability during temperature fluctuations (as depicted in **Figure 2**). Additionally, cutouts around the optics bench provide space for thermal straps, allowing for the connection of the optics bench's outer diameter to the cold plate without interfering with the placement of the 120 K radiative shell (as illustrated in **Figure 1**).

We make use of aluminum standoff spacers under all the bolt interfaces, to compensate for the CTE difference between the titanium 6Al-4V parts and the 18-8 stainless steel hardware and maintain correct bolt tension under cooling.

2.2 Optical Redesign

The thermal analysis described in Section **2.1** also identified an issue with the 90° OAP used in the original design.[2] The 90° OAP substrate is an aluminum cylinder with a diameter of 25 mm, with the tangential optical surface defined by a cut at 45° through the cylinder. This 45° angle means that between the upper and lower edge of the optical surface there is a difference of ~ 18 mm in the thickness of the aluminium substrate, which would produce a significant distortion on the order of 80 μm in the surface of the sensitive collimating optic. To address this, we redesigned the spectrograph to make use of a 45° OAP, cutting the tangential angle in half. This decreased the distortion from CTE by a factor of 1.85. But more significantly, the tangential angle effects the sensitivity of the OAP to misalignment (see our previous paper, Bernard et al 2022,[2] for more details on how OAP working angle effects alignment sensitivity). The change in working angle to 45° from 90° increased our error budget by a factor of 2.4, both benefiting our tolerance to CTE distortion and relaxing our alignment tolerance to 28 arcminutes. This relaxed angular tolerance also increased the usable field of view of the spectrograph, relaxing the acceptable input ray location to ±1.5 mm of the field stop center, allowing diffraction-limited performance through the entire field stop.

The 90° angle between the input beam and the collimated beam (see **Figure 1**) is important for the alignment procedure (**Section 4.3**). To ensure this angle, we combined the field stop and fold mirrors 1 and 2 into a single, precision-machined tri-mount that redirects the input beam by 45°. When the spectrograph is properly aligned, the tri-mount combines with the new OAP 1 to maintain the 90° angle of the collimated beam.

2.3 Thermal Modeling

The FEM focuses on assessing stress at the interface between the optics bench and cold plate, specifically examining the impact of the mismatched CTE. The model is configured with an initial stress-free temperature of 20°C (293 K) and a final settling temperature of −153°C (120 K), representative of typical operational conditions for the spectrograph. The analysis revealed a peak stress of 455 MPa at a joint within the flexures (see **Figure 3**). Titanium 6Al-4V, the material of the optics bench, possesses a yield strength of 830 MPa and an ultimate yield strength of 900 MPa. In cases where stress exceeds 830 MPa but remains below 900 MPa, the flexures are likely to bend without returning to their nominal position. However, if stress surpasses 900 MPa, the flexures risk catastrophic failure. With a peak stress of 455 MPa, we observe a safety margin of 1.82, comfortably meeting the minimum requirement of 1.2 for safety margins.

3. LABORATORY DEMONSTRATIONS

3.1 Collimated light source measurements

Our laboratory testing setup makes use of a well-collimated light source and a shear plate interferometer. A detailed description of shear plate interferometers can be found in Riley and Gusinow 1977;[6] here we provide here a brief summary of shear plate functions relevant to our application.

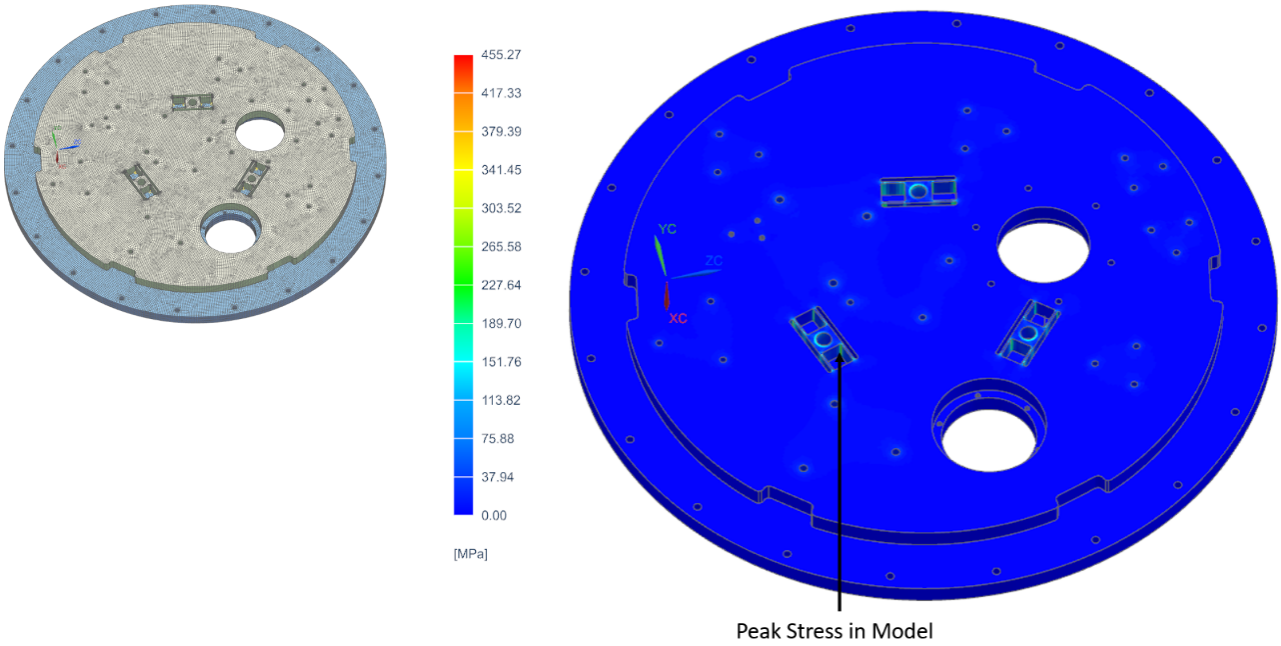

Figure 3: Optics Bench Flexure Stress Analysis.
Left Image of the Finite Element Model (FEM). **Right** Image of the results of the thermal analysis, showing peak stress at 455.27 MPa at a joint in the flexure.

A shear plate interferometer is an optical glass plane plate which operates by overlapping the beams reflected from both surfaces of the plate. With monochromatic light (λ), the thickness of the plate (the *shear distance*) introduces a phase difference between the beam paths, causing interference in the overlapping beams; a slight wedge angle in the plate introduces a sinusoidal modulation in the interference, which appears as a fringe pattern. This sinusoidal fringe pattern is a function of the local radius of curvature of the wavefront, enabling a direct measurement of wavefront error.

The intensity of the fringe pattern is given by $I = \sin^2 \frac{1}{2}\Phi$. In the case of a spherical wavefront, the phase difference Φ is given by

$$\Phi(x, y) = \frac{2\pi}{\lambda}\left(\theta\left(1 - \frac{R_s}{R_c}\right)y + \frac{S}{R_c}x\right) \tag{2}$$

where θ is the beam angle difference due to the wedge, R_c is the radius of curvature of the wavefront, R_s is the distance from the shear plate to the observation plane, S is the shear distance, y is the direction of the wedge, and x is the direction perpendicular to the wedge. Note how in the limit of $R_c \to \infty$ (a flat wave-front, i.e., collimated light), the phase difference collapses to $\Phi = \frac{2\pi}{\lambda}\theta y$, meaning in the case of collimated light the shear pattern produces parallel fringes exactly perpendicular to the wedge. Also note that for spherical light, the phase equation is linear in the $x - y$ plane, so that as the light deviates from a perfect plane wave and gains a radius of curvature the fringes remain parallel but gain a slope, changing angle with respect to the direction of the shear. The angle (ϑ) of the fringe pattern produced by **Equation 2** is given by

$$\tan\vartheta = \frac{-\theta S\,(1 - R_s/R_c)}{R_c},\ R_s << R_c \tag{3}$$

This means the collimation of a beam of light can be directly measured with high accuracy by simply measuring the angle of the fringe pattern.

The shear plate interferometer can also be used to measure abberations. Optical aberrations produce deviations in the wave-front, which appear as non-linear curves in the fringe pattern described above. The patterns

produced by large abberations are beyond the scope of this paper, but for small aberrations the fringe pattern is an approximately linear projection of the two wavefront's interference pattern, with the peak-to-peak of the pattern corresponding to one wavelength λ. The error in the wavefront can be estimated by counting the number of fringes in the deviation, with one fringe equal to $\frac{1}{2}\lambda$. This makes the shear plate interferometer convenient for estimating small wavefront errors as a fraction of λ.

3.2 Parts Acceptance Testing

We test the precision of our optical components using a combination of a HeNe laser source ($\lambda = 633$ nm) and optics to produce a precision light source, with measurements provided by a 25 mm shear plate interferometer. The optics have two configurations, once producing collimated light and the other producing focused light. We used the collimated mode to test flat optics, such as the fold mirror and the dichroics, by measuring the shear plate interference pattern before and after the flat and comparing the differences (if any exist). For testing powered optics we used focused mode, using the OAPs to collimate the focused source and then measuring how well-collimated the output is using the shear plate.

While our design criteria wavelength is 1.0 μm, the 633 nm light of the laser is not only easier to use in the laboratory but is more sensitive to error than infrared light. We choose an optical surface quality tolerance of $\lambda/2$, which translates to an accuracy of $> \lambda/4$ for the Nyquist-sampled spectrograph wavelengths. Additionally, we test the optics with a 25 mm diameter beam, instead of the actual instrument's 8 mm, further increasing our test's sensitivity to error over real operations.

We found wavefront error to be $< \lambda/4$ for all optics, with the exception of the 45° OAP where we found a wavefront error of $\sim \lambda/3$ (see **Figure 4**). We note that the 45° OAP was tested with a F/4 beam, so while this larger error could be due to optic surface quality, it could also be the limitations of our laser source optics; limitations that would not affect the other, slower-beam tests. We also note that our 25 mm beam will detect defects in the edge of the mirror, which will not affect the 8 mm beam of the operating spectrograph. Regardless, all optics exceed our criteria of $\lambda/2$

We used a straight-edge and a precision square to check the accuracy of the machined optical mounts and the optical bench, making use of a feeler gauge to measure any inaccuracy. All mounts were within 0.0015 inches (38 μm) of design on critical surfaces, with the exception of some slight warping on the base of the OAP mount which we corrected with a 0.002 in shim. We measured the optical bench as flat within 0.007 in (178 μm) over the 11 inch (280 mm) diameter.

As a final test, we made a mock assembly of the spectrograph parts on the optical bench, and verified system throughput with HeNe laser. (see **Figure 5**.)

4. INSTRUMENT ASSEMBLY AND ALIGNMENT

4.1 Cyrostat Radiative Link

Titanium 6Al-4V provides great stability, but unfortunately has poor thermal conductivity, making stable cooling a challenge. To mitigate this, we decided to make use of a high emissivity coating consisting (**Figure 8**) of Aeroglaze 9929 epoxy primer and Aeroglaze Z306 topcoat, enabling efficient radiative cooling in addition to what is provided by the cold plate and copper straps. In preparation for coating process we thoroughly cleaned the machined parts with degreaser and isopropanol, baked the parts in a vacuum oven, and masked all mechanical interface surfaces to preserve the machined tolerances. We worked with an industry contractor for sample testing and coating. A matching coating on the cyrostat inner shell radiatively links the spectrograph to the cryostat, which in combination with the large surface area provides a significant amount of cooling. See Kleyheeg et al. for details on the spectrograph cyrostat.[3]

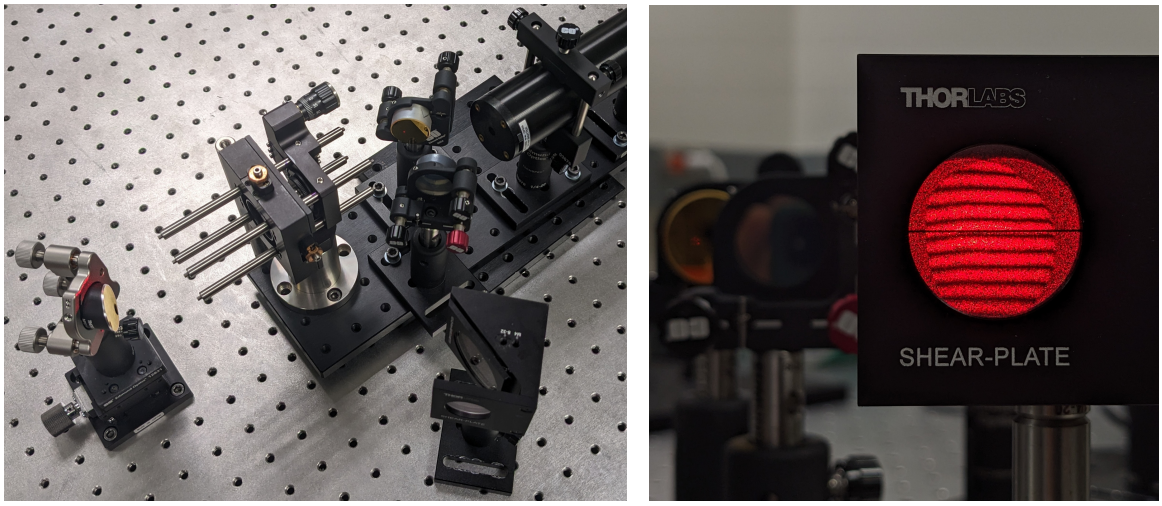

Figure 4: Example of the setup used to verify the performance of optical components, in this case the 45° OAP. **Left:**Isometric top-down view of testing the 45° OAP, mounted to a 1-inch grid optical table. We use a microscope objective lens to direct light onto the focal plane of the OAP, which the OAP then collects and collimates. Note how compact the measurement system is. **Right:** Image of the shear plate interference pattern produced by the collimated beam of the 45° OAP during the test. This provides a direct measurement of wavefront error, which we use to infer optic performance, which in this case is approximately $\lambda/3$.

4.2 Alignment Criteria

In our previous paper,[2] we provided alignment the alignment criteria of the spectrograph. Here we update the criteria of OAP 1. OAP 1 remains the most sensitive optic in the assembly, and as described in our previous paper drives the tolerances of EXCITE's spectrograph.

Our criteria is maintaining diffraction-limited performance, which we for the purposes of alignment we define as a Strehl ratio of 0.8 at a wavelength (λ) of 1.0 µm. In our case, the secondary mirror obscures 38% of the telescope aperture. With this .38 central obscuration, a Strehl ratio of 0.8 corresponds to a defocus d of

$$d = 2.41\,\lambda\,F^2 \tag{4}$$

where F is the telescope focal ratio.[7] As we discuss in Bernard et al 2022,[2] OAP misalignment appears as an effective defocus, which can be translated into an angular misalignment after accounting for the working angle of the OAP. The angular misalignment (δ) for an OAP with focal length f and working angle θ is given by

$$\delta = \frac{d}{f\,\tan\frac{\theta}{2}} = \frac{2.41\,\lambda\,F^2}{f\,\tan\frac{\theta}{2}} \tag{5}$$

For OAP 1, which receives the $f/12$ ($F = 12$) beam of the telescope, this produces a maximum alignment tolerance of ±28 arcminutes.

4.3 Optics Alignment

OAPs asymmetric nature makes them challenging to align. They must be aligned in 6 degrees of freedom: x, y, z, rotation in the x-y plane (*roll*), rotation in the x-z plane (*yaw*), and rotation in the y-z plane (*pitch*), where z is the axis along the beam path, x is the horizontal perpendicular axis, and y is the vertical perpendicular axis. These axes are degenerate, meaning any particular aberration could be due to misalignment in one of two axis, or a combination of misalignment in both. To break this degeneracy, we use the mechanical design of the spectrograph to eliminate degrees of freedom wherever possible.

We use the same HeNe laser and shear plate used for acceptance testing to align the spectrograph. For alignment, we secured the spectrograph to an optical bench, with the entrance aperture aligned to the optical

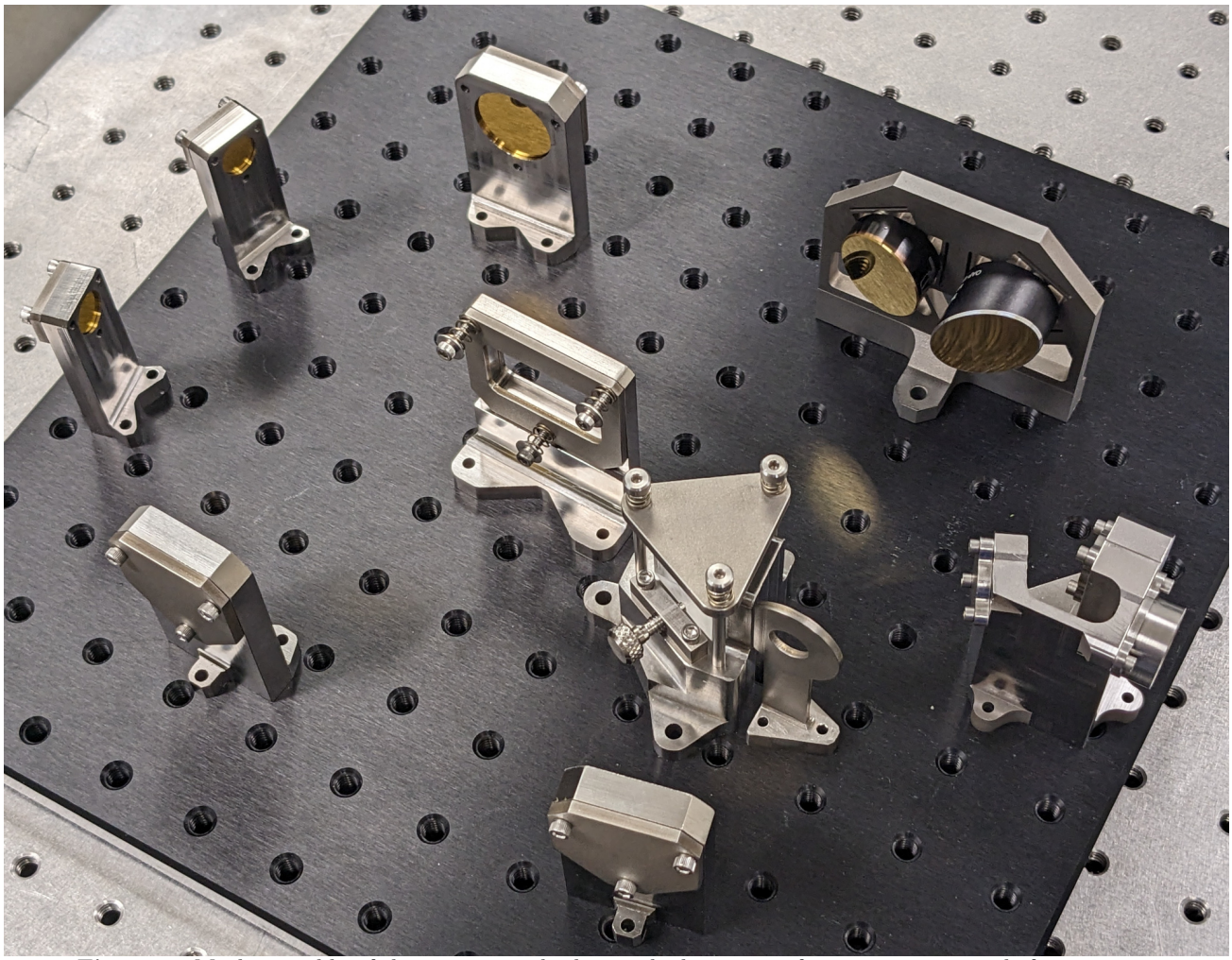

Figure 5: Mock assembly of the spectrograph, during the last stage of acceptance testing before coating.

grid. We mounted the laser source to an optical island, allowing us to move the light source while maintaining alignment relative to the bench. We made use of two source modes, a collimated light mode and an simulated single ray mode (described below). We developed a third mode, the focused input configuration we made use of in acceptance testing, but found it unnecessary for our 28 arcminute alignment criteria.

For rough alignment, we take advantage of the 100 µm entrance slit to filter the 633 nm laser beam to an approximation of a single chief ray (the *simulated chief ray*). The diffraction pattern produced by the slit tells us the orientation of the slit, which we adjust to be horizontal (ensuring a vertical slit). We then center the core of the diffraction pattern beam on each optic in turn, ensuring the beam is level throughout the system and centered on each optic.

Once the spectrograph is roughly aligned, we align the critical optic, the 45° OAP that collimates the telescope beam (OAP 1). To align OAP 1, we take advantage of the rotational symmetry of the collimation side of the optic. When collimated light is directed into OAP 1, operating the optic in reverse (see **Figure 6**), the x-y-z axes are eliminated as variables (as collimated light is translation-independent). Any *roll* misalignment will not affect the focus, but will direct the focus light at some angle; when the focused beam projection is horizontal, the *roll* axis is aligned to 0°. We control the *pitch* angle with the OAP mount, which was measured as 90° with precision square during acceptance testing and verified with the simulated chief ray. To control the *yaw* angle, we take advantage of the tri-mount's 45° beam folding: if the reverse operation emits focused light through the field stop at exactly 90° relative to the collimated beam, we know the OAP 1 is aligned to 45° working angle.

There is a degeneracy between the *yaw* alignment and the x-axis alignment; any misalignment in the *yaw* can be compensated for by translation in the x direction, at the cost of producing astigmatism and changing the angle of the output beam. We break this degeneracy by comparing the angle of the reverse operation output beam to the angle of the simulated chief ray. The optical island enabled us to switch between chief ray mode and reverse operation mode while maintaining alignment, using precision stops mounted to the optical bench to ensure a mechanical $90° \pm 1.6'$ between the modes. This allowed us to iterate between modes until we achieved alignment. Using this procedure, we achieved an alignment of 12 arcminutes or better, well under our budget of 28 arcminutes, with the primary limiting factor being the accuracy of the measurement of the beam angle between the two modes. Note that we have not reached the accuracy limit of our light source, 1.6 arcminutes, meaning we have room to improve the OAP 1 alignment should future engineering tests find any unexpected sources of error.

Finally, we adjust focus (z-axis alignment) by maximizing the output through the field stop, taking advantage of the fact that as this is effectively a slit-less spectrometer, the telescope focus can be used to adjust spectrograph focus alignment during flight. Alignment of OAP 1 in the y-translation (cross-dispersion, a.k.a., slit direction) is non-critical, with the entire field stop being usable.

OAP 2 is co-mounted with OAP 1, with their co-alignment ensured by the machined surface and precision pins. This co-mounting ensures OAP 2 shares alignment with OAP 1 in all axes, except for *roll*. As mentioned earlier, a misalignment in *roll* does not affect the Strehl ratio but merely tilts the beam path. Additionally, OAP 2 has a large depth of focus ($\sim \pm 600$ µm) which prevents any aberration due to tilt of the focal plane. This makes OAP 2 simple to align by leveling its output beam, with alignment in all other degrees of freedom constrained by the alignment of OAP 1. (See Bernard et al 2022[2] for a more detailed description of the relaxed alignment tolerance of OAP 2.)

All fold mirrors and the prism are aligned by centering and leveling the simulated chief ray, with appropriate calculated offsets to account for the prism dispersion. (**Figure 7**)

5. CONCLUSIONS AND FUTURE WORK

We have identified issues with the preliminary design of the EXCITE spectrograph related to thermal stability and addressed them via model-driven design changes, including the incorporation of mechanical flexures, changing the optical bench and mount material to titanium 6Al-4V, and a redesign of the collimating OAP. We have mitigated the downsides of these changes through model-driven design, while also incorporating alignment procedure concerns into the mechanical and optical design.

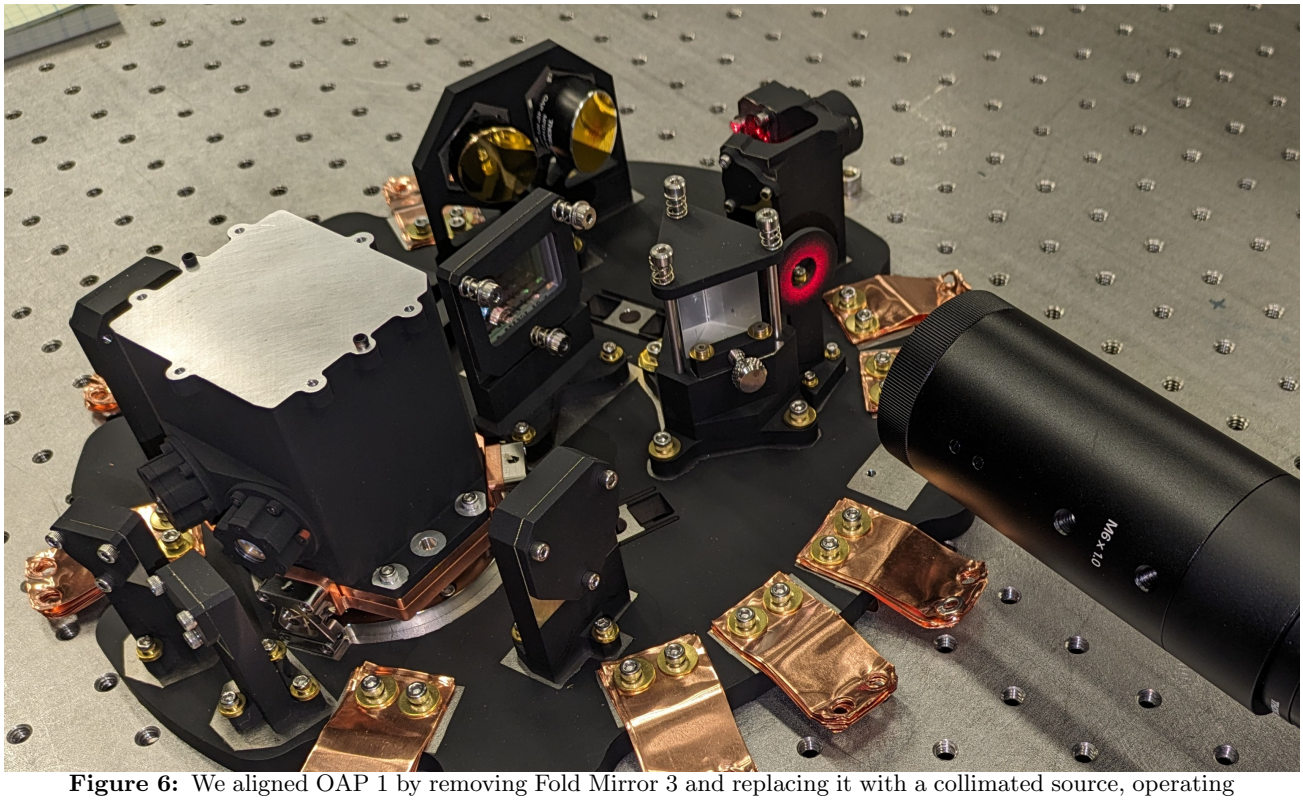

Figure 6: We aligned OAP 1 by removing Fold Mirror 3 and replacing it with a collimated source, operating the OAP in reverse. In this configuration, we were able to achieve the target alignment of 28 arcminutes. As the two OAPs are co-mounted, this also aligns the lighter tolerance OAP 2.

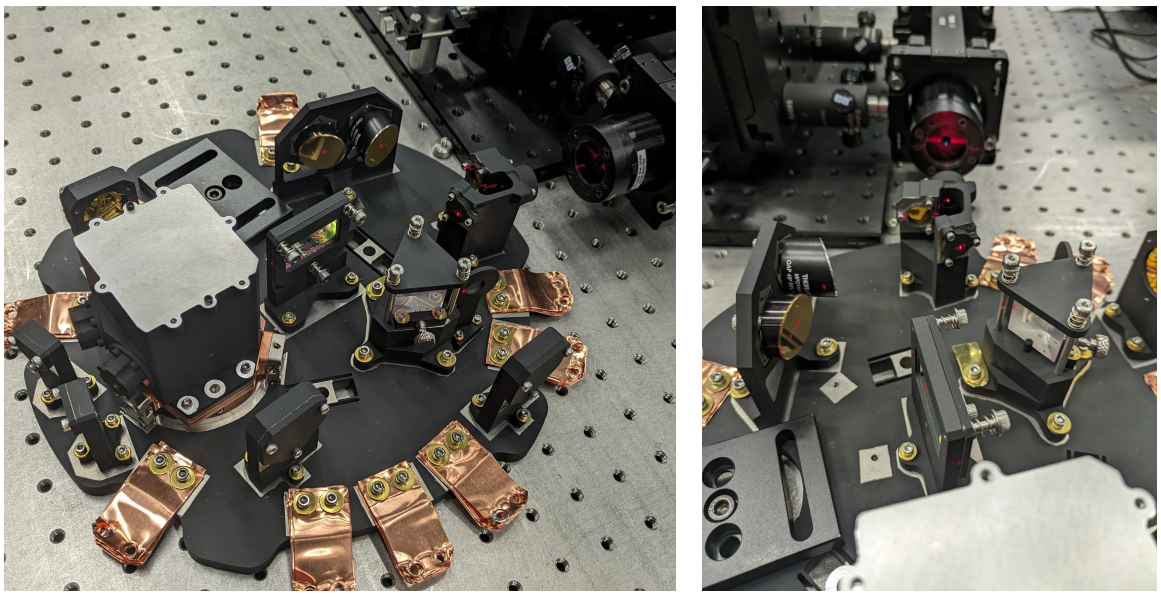

Figure 7: After aligning the 45° OAP, we re-installed Fold Mirror 3. We aligned a laser beam along the optical axis, simulating a chief ray, which we then used to steer the beam path using the fold mirrors.

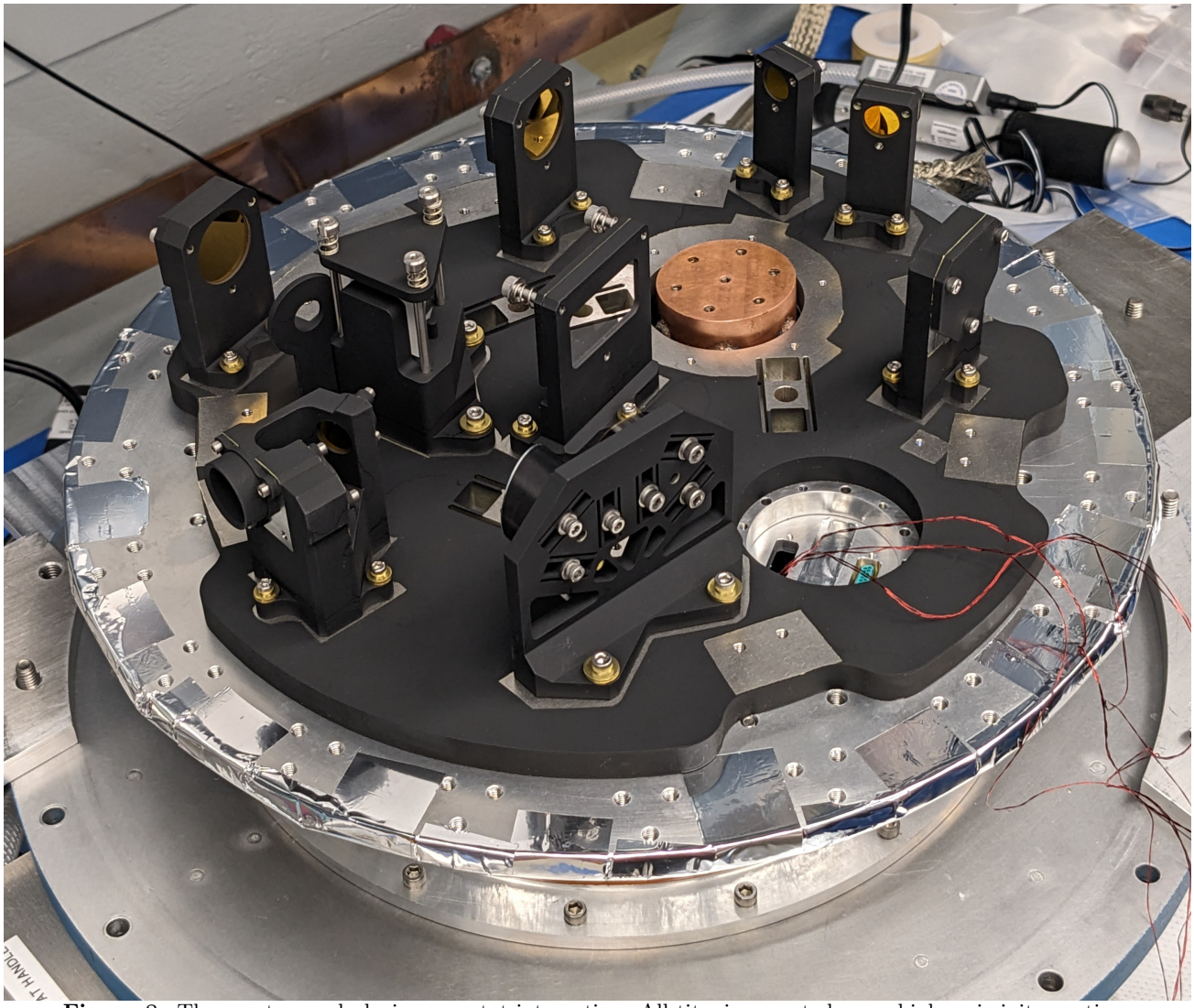

Figure 8: The spectrograph during cryostat integration. All titanium parts have a high emissivity coating, radiatively linking the spectrograph with the cryostat shell to mitigate the low thermal conductivity of the titanium. In this image we use brass stand-offs under the bolt heads; we later swapped these to aluminum stand-offs.

This has enabled us to construct and align the EXCITE spectometer at room temperature, with alignment verified through laser measurements to an accuracy of > 12 arcminutes and thermal simulations indicating it will retain alignment within acceptable tolerance at operating temperature. Currently, we are measuring spectrograph signal throughput at both room temperature and the 120 K operating temperature, to verify that alignment is retained during cooldown. After the completion of throughput testing, the spectrograph cryostat will be integrated with the EXCITE telescope and gondola, in preparation for an engineering test flight of the EXCITE mission from Ft Sumner, New Mexico USA in Fall 2024.

ACKNOWLEDGMENTS

This work is supported by NASA award 18-APRA18-0075 selected under NASA Research Announcement NNH18ZDA001N, Research Opportunities in Space Science – 2018 (ROSES-2018). Work by Kyle Helson is supported by NASA under award number 80GSFC21M0002.

REFERENCES

[1] P. C. Nagler, L. Bernard, A. Bocchieri, N. Butler, Q. Changeat, A. D'Alessandro, B. Edwards, J. Gamaunt, Q. Gong, J. Hartley, K. Helson, L. Jensen, D. Kelly, K. Klangboonkrong, A. Kleyheeg, N. Lewis, S. Li, M. Line, S. Maher, R. McClelland, L. Miko, L. Mugnai, B. Netterfield, V. Parmentier, E. Pascale, J. Patience, T. Rehm, J. Romualdez, S. Sarkar, P. Scowen, G. Tucker, A. Waczynski, and I. Waldmann, "The EXoplanet Climate Infrared TElescope (EXCITE)," in *Ground-based and Airborne Instrumentation for Astronomy IX*, C. J. Evans, J. J. Bryant, and K. Motohara, eds., p. 31, SPIE, (Montréal, Canada), Aug. 2022.

[2] L. Bernard, L. Jensen, J. Gamaunt, N. Butler, A. Bocchieri, Q. Changeat, A. D'Alessandro, B. Edwards, Q. Gong, J. Hartley, K. Helson, D. Kelly, K. Klangboonkrong, A. Kleyheeg, N. Lewis, S. Li, M. Line, S. Maher, R. McClelland, L. Miko, L. Mugnai, P. Nagler, B. Netterfield, V. Parmentier, E. Pascale, J. Patience, T. Rehm, J. Romualdez, S. Sarkar, P. Scowen, G. Tucker, A. Waczynski, and I. Waldman, "Design and testing of a low-resolution NIR spectrograph for the EXoplanet Climate Infrared TElescope," in *Ground-based and Airborne Instrumentation for Astronomy IX*, C. J. Evans, J. J. Bryant, and K. Motohara, eds., p. 80, SPIE, (Montréal, Canada), Aug. 2022.

[3] A. Kleyheeg, L. Bernard, A. Bocchieri, N. Butler, Q. Changeat, A. D'Alessandro, B. Edwards, J. Gamaunt, Q. Gong, J. Hartley, K. Helson, L. Jensen, D. Kelly, K. Klangboonkrong, E. Leong, N. Lewis, S. Li, M. Line, S. Maher, R. McClelland, L. Miko, L. Mugnai, P. Nagler, C. B. Netterfield, V. Parmentier, E. Pascale, J. Patience, T. Rehm, J. Romualdez, S. Sarkar, P. Scowen, G. Tucker, A. Waczynski, and I. Waldmann, "Integration and testing of a cryogenic receiver for the Exoplanet Climate Infrared Telescope (EXCITE)," in *Ground-based and Airborne Instrumentation for Astronomy X*, J. R. Vernet, J. J. Bryant, and K. Motohara, eds., p. 140, SPIE, (Yokohama, Japan), July 2024.

[4] L. J. Romualdez, L. Bernard, A. Bocchieri, N. Butler, Q. Changeat, A. D'Alessandro, B. Edwards, J. Gamaunt, Q. Gong, J. W. Hartley, K. Helson, L. Jensen, D. P. Kelly, K. Klangboonkrong, A. Kleyheeg, E. Leong, N. Lewis, S. Li, M. Line, S. Maher, R. McClelland, L. R. Miko, L. V. Mugnai, P. C. Nagler, C. B. Netterfield, V. Parmentier, E. Pascale, J. Patience, T. Rehm, S. Sarkar, P. Scowen, G. S. Tucker, A. Waczynski, and I. Waldmann, "The EXoplanet Climate Infrared TElescope (EXCITE): Gondola Pointing & Stabilization Qualification," in *Ground-based and Airborne Telescopes X*, H. K. Marshall, J. Spyromilio, and T. Usuda, eds., p. 136, SPIE, (Yokohama, Japan), Aug. 2024.

[5] P. R. Yoder, *Mounting optics in optical instruments*, SPIE, Bellingham, 2nd. ed ed., 2008. OCLC: 1416086314.

[6] M. E. Riley and M. A. Gusinow, "Laser beam divergence utilizing a lateral shearing interferometer," *Applied Optics* **16**, p. 2753, Oct. 1977.

[7] V. N. Mahajan, "Strehl ratio for primary aberrations: some analytical results for circular and annular pupils," *Journal of the Optical Society of America* **72**, p. 1258, Sept. 1982.